CrossMark

Modeling Two- and Three-Stage Oxygen Tracer Experiments during High-Temperature Oxidation of Metals with a High Oxygen Solubility

Benoît Mazères[1,2,5] · Clara Desgranges[2,4] · Caroline Toffolon-Masclet[3] · Daniel Monceau[1]

Abstract The numerical tool EKINOX-Zr has been upgraded to simulate oxygen tracer experiments during the high-temperature oxidation of a metal with a high oxygen solubility limit. The penetration of ^{18}O tracer is calculated during the dynamic evolution of the $ZrO_{2-x}/\alpha_{Zr(O)}/\beta_{zr}$ system. The numerical approach allows to explicitly take into account the variation of the tracer diffusion coefficient through the oxide scale as a function of the vacancy concentration. A classical two-stages $^{16}O_2/^{18}O_2$ tracer experiment has been simulated. It is shown that a classical fitting procedure on the ^{18}O concentration profile obtained for short-time experiments leads to the identification of the oxygen chemical diffusion coefficient. The second type of tracer experiment is proposed using a three-stages $^{16}O_2/^{18}O_2/^{16}O_2$

✉ Daniel Monceau
   daniel.monceau@ensiacet.fr

   Benoît Mazères
   benoit.mazeres@gpseo.fr

   Clara Desgranges
   clara.desgranges@safrangroup.com

   Caroline Toffolon-Masclet
   caroline.toffolon@cea.fr

1   CIRIMAT, Université de Toulouse, CNRS, INPT, UPS, ENSIACET, 4 Allée Emile Monso, BP-44362, 31030 Toulouse Cedex 4, France

2   DEN-Service de la Corrosion et du Comportement des Matériaux dans leur Environnement, CEA, Université Paris-Saclay, 91191 Gif-sur-Yvette, France

3   DEN-Service de Recherches Métallurgiques Appliquées, CEA, Université Paris-Saclay, 91191 Gif-sur-Yvette, France

4   Present Address: SAFRAN Tech, rue des Jeunes Bois, 78772 Magny-les-Hameaux, France

5   Present Address: CU GPS&O, Immeuble Autonéum, Rue des Chevries, 78410 Aubergenville, France

oxidation. It allows the direct estimation of the diffusion coefficient from the transport of ^{18}O peak in the growing oxide scale.

Keywords Zirconium · Tracer experiment · ^{18}O · Numerical modeling · Diffusion

List of symbols

a_i	Chemical activity of the specie i
R	Universal gas constant
C_O	Oxygen concentration
R_{18}	Volume ratio of the mix gas $^{18}O_2/^{16}O_2$
D_O^p	Oxygen diffusion coefficient in the metal
T	Temperature
D_{ox}^q	Oxygen diffusion coefficient in the oxide
X_i^r	Concentration of the specie i in the slab r
e	Elementary charge
a	Relative electric charge of the oxygen vacancies
f_O	Correlation factor
Δt	Numerical time step
J_i^r	Flux of the specie i from the slab r to the slab $r+1$
μ_O	Chemical potential of oxygen
K	Equilibrium constant
σ_k	Electrical conductivity of the specie k
L_{ij}	Crossed diffusion coefficient
Ω^r	Molar volume of the slab r

Introduction

Oxygen tracer (O-tracer) experiments are one mode to measure oxygen diffusion coefficients and/or to understand the growth mechanisms of an oxide scale. Nowadays, these experiments consist in a two-stage oxidation. The first stage is generally performed under a natural oxygen atmosphere (majority of $^{16}O_2$) while the second stage is carried out under an $^{18}O_2$-enriched atmosphere. Then, SIMS, RBS or NRA can be used to measure the distribution profile of each isotope and extract the expected information.

In order to analyze the isotopic distribution profiles, an analytical theory of O-tracer penetration in two-stage oxidation experiments has been formalized by Mishin and Borchardt [1]. This theory gives the equations for the O-tracer penetration through both grain boundaries and sublattice diffusion in a growing oxide layer, with both the anionic and the cationic transports. Hence, their work has guided numbers of studies concerning O-tracer experiments to correctly define the time ratio between $^{18}O_2$ and $^{16}O_2$ sequences [2]. Despite this very useful approach, their analytical theory suffers from several restrictions. First, it is not possible to handle neither a temperature transient oxidation nor a triple sequence

$^{16}O_2/^{18}O_2/^{16}O_2$. Furthermore, it is assumed in their work that the oxide scale growth kinetics is fully controlled by the fluxes in the oxide because oxygen dissolution in the metal can be often neglected.

In this study, the aim was to measure the oxygen diffusion coefficient in specific phases of the zirconium/zirconia system. Zirconium, as titanium and hafnium, has a very high oxygen solubility limit [3]. Thus, in order to analyze the isotope penetration profiles in these specific systems, it was required to develop a numerical model able to calculate ^{16}O and ^{18}O penetration for the particular case of the oxygen penetration in the underlying metal. To do that, EKINOX-Zr numerical model [4–6] has been upgraded in order to calculate the isotopic penetration. Formerly, the EKINOX-Zr model was developed to simulate the high-temperature (HT) oxidation of zirconium alloys. Hence, this numerical model is able to calculate the growth of both the oxide scale and the $\alpha_{Zr}(O)$ phase additionally to the penetration of oxygen. To calculate the isotope penetration, ^{18}O was added to the system of equations to be solved, and it was assumed that ^{16}O and ^{18}O were two distinct species that diffuse independently but on the same sublattice and under the same driving forces.

This paper deals with the development of theoretical approach to formalize the flux equations of isotopic tracers in the oxide scale with anionic transport. Then, its appliance with the EKINOX-Zr numerical model was tested.

Formulation of the Tracer Diffusion Equations

Theoretical Approach

In this part, the equations of the fluxes of $^{18}O^{2-}$ and $^{16}O^{2-}$ species in the oxide scale are detailed. They lead to the numerical model presented in the next part.

The electrochemical potential $\tilde{\mu}_i$ of a given specie i[1] is linked to its chemical activity a_i by the Eq. (1):

$$\forall i \in \{16; 18\}, \tilde{\mu}_i = \mu_i + \alpha e \phi^{ox} = \mu_i^0 + RT\ln(a_i) + \alpha e \phi^{ox} \tag{1}$$

where ϕ^{ox} is the local electrostatic potential, e is the elementary charge, and α is the charge of the specie i. Let us assume the case of an oxygen deficient n-type semiconducting oxide.

In this case, there is a transport of oxygen anions and electrons in the oxide due to the electrochemical potential gradient across the oxide scale. The diffusion of charged particles gives rise to partial current densities of oxygen and electrons that leads to a total current i_{tot} [7, 8]. Because of the electroneutrality of the overall oxide layer, $i_{tot} = 0$, the flux of specie i can be expressed as follows:

---

[1] In order to clarify the notations, all the terms "A" linked to ^{18}O will be mentioned as A_{18}. The same convention is followed for the terms linked to the ^{16}O. When a generic term is used, it will be mentioned as A_i.

$$\forall i \in \{16; 18\}, J_i = -\frac{D_i . C_i}{RT} \left[\frac{\mathrm{d}\mu_i}{\mathrm{d}x} + a_i e \frac{\mathrm{d}\phi^{\mathrm{ox}}}{\mathrm{d}x} \right] \tag{2}$$

By using the Wagner model of oxidation (see [8]), with the hypotheses of a semiconducting oxide in which the electronic defects diffuse much faster than the anions and with the assumption of the local equilibrium across the oxide, it is possible to write the flux equations of the diffusing species in the oxide scale as a function of the oxygen activity gradient across the oxide scale:

$$\forall i \in \{16; 18\}, J_i = -D_O \cdot \left(\frac{\mathrm{d}C_i}{\mathrm{d}x} - C_i \cdot \frac{\mathrm{d}ln a_O}{\mathrm{d}x} \right) \tag{3}$$

In the following, the case of an oxide scale that grows via anionic transport[2] only by a vacancy mechanism is considered. At the oxide/gas interface, the oxygen adsorption is possible thanks to the annihilation of anionic vacancies following the Eq. (4) (using Kröger-Vink notations):

$$1/2 O_2 + V_O^{a\bullet} + \alpha e^- = O_o^\times \tag{4}$$

The transport mechanism for anions can be described as the transport in the opposite way of anionic vacancies $V_O^{a\bullet}$; anionic vacancies are created at the metal/oxide interface and annihilated at the oxide/gas interfaces. It is possible to write the equilibrium constant K of the chemical reaction at the oxide/gas interface (Eq. 5):

$$K = \frac{1}{a_O n^\alpha \left[V_O^{\alpha\bullet} \right]} \tag{5}$$

Expressions of the chemical activities a_O, a_{16}, and a_{18} can be deduced from the Eq. (5), using the local electroneutrality to remove the electron concentration n from the equation:

$$a_O = \frac{1}{a^\alpha \left[V_O^{\alpha\bullet} \right]^{(1+\alpha)} K} \tag{6}$$

$$\forall i \in \{16; 18\}, a_i = \frac{C_i}{C_O} a_O \tag{7}$$

Following Eqs. (1), (6), and (7), the expression of the chemical potential μ_{16}[3] is given by:

$$\mu_{16} = \mu_{16}^0 + RT \left(\ln\left(\frac{C_{16}}{C_O} \right) - (1+\alpha) \left(\ln\left(\left[V_O^{\alpha\bullet} \right] - \ln(Ka^\alpha) \right) \right) \right) \tag{8}$$

---

[2] In case of an anionic transport in the oxide scale, the anion flux is predominant, whereas the cation flux is negligible.

[3] The same development can be done for μ_{18}.

Considering that, in the oxide scale, the anionic vacancies and anions are complement one another in the anionic sublattice: $C_O = 1 - [V_O^{a\bullet}]$, and that Ka^α is a constant across the scale, an expression of $\nabla\mu_{16}$ can be deduced from Eq. (8):

$$\nabla\mu_{16} = RT\left(\frac{\nabla C_{16}}{C_{16}} - \left(\frac{1+a}{[V_O^{\alpha\bullet}]} - \frac{1}{1-[V_O^{\alpha\bullet}]}\right)\nabla C_O\right) \tag{9}$$

According to the thermodynamic of irreversible processes (e.g. [9]), the flux J_{16} of $^{16}O^{2-}$ and the flux J_{18} of $^{18}O^{2-}$ can be expressed with the crossed diffusion coefficients and the chemical potentials of each specie as given in Eq. (10):

$$\forall\{i;j\} \in \{16;18\}|i \neq j, J_i = -L_{ii}\nabla\mu_i - L_{ij}\nabla\mu_j \tag{10}$$

Knowing that $\frac{L_{OO}}{C_O} = \frac{L_{1616}}{C_{16}}$, it can be assumed that: $D_O = \frac{RT}{C_O}L_{OO}f_O$. It is chosen to fix that $f_O = 1 - \frac{C_O L_{1618}}{C_{18} L_{OO}}$ and $L_{1618} = 0$, thus $f_O = 1$. Then, by a combination of the Eqs. (9) and (10), one can obtain an expression of the flux J_{16} and J_{18}:

$$\forall i \in \{16;18\}, J_i = -D_O\nabla C_i - D_O C_i\left(\frac{1+\alpha}{[V_O^{\alpha\bullet}]} - \frac{1}{1-[V_O^{\alpha\bullet}]}\right)\nabla C_O \tag{11}$$

In the flux expression (Eq. 11), we can find two distinct parts in the RHS. The first part, $-D_O\nabla C_a$, corresponds to the diffusion (Brownian motion) while the second part, $-D_O C_i\left(\frac{1+\alpha}{[V_O^{\alpha\bullet}]} - \frac{1}{1-[V_O^{\alpha\bullet}]}\right)\nabla C_O$, is the transport induced by the gradient of the electrochemical potential. Considering that $C_O D_O = [V_O^{\alpha\bullet}]D_{V_O^{\alpha\bullet}}$ and defining $\gamma = \frac{[V_O^{\alpha\bullet}]}{(1+\alpha)(1-[V_O^{\alpha\bullet}])}$ and $\tau_i = \frac{C_i}{C_O}$, one can express the fluxes J_{16} and J_{18} as given by Eq. (17):

$$\forall i \in \{16;18\}, J_i = -\gamma(1+\alpha)D_{V_O^{\alpha\bullet}}\nabla C_i - \tau_i(1-\gamma)(1+\alpha)D_{V_O^{\alpha\bullet}}\nabla[V_O^{\alpha\bullet}] \tag{12}$$

In the case where $[V_O^{\alpha\bullet}] \ll 1 \Rightarrow \gamma \approx \frac{[V_O^{\alpha\bullet}]}{1+\alpha}$, one can simplify the Eq. (12):

$$J_{18} = -[V_O^{\alpha\bullet}]D_{V_O^{\alpha\bullet}}\nabla C_{18} - \tau_{18}(1+\alpha)D_{V_O^{\alpha\bullet}}\nabla[V_O^{\alpha\bullet}] \tag{13}$$

It is possible to obtain an expression of $\tilde{D}_O$ (the chemical diffusion coefficient of oxygen) from the Eq. (13):

$$J_{18} = -[V_O^{\alpha\bullet}]D_{V_O^{\alpha\bullet}}\nabla C_{18} - \tau_{18}(1+\alpha)D_{V_O^{\alpha\bullet}}\nabla[V_O^{\alpha\bullet}] = -\tilde{D}_O\nabla C_{18}$$

$$\Rightarrow \tilde{D}_O = \left(1 + \left(\frac{1+\alpha}{[V_O^{\alpha\bullet}]} - \frac{1}{C_O}\right)C_{18}\frac{\nabla[V_O^{\alpha\bullet}]}{\nabla C_{18}}\right)\frac{[V_O^{\alpha\bullet}]}{C_O}D_{V_O^{\alpha\bullet}} \tag{14}$$

Knowing that $(1+\alpha)D_{V_O^{\alpha\bullet}}\nabla[V_O^{\alpha\bullet}] = -J_{V_O^{\alpha\bullet}} = J_O$, the Eq. (18) becomes:
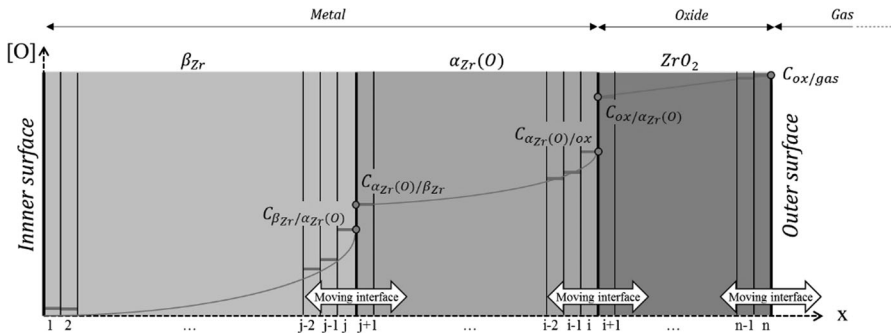
Fig. 1 Schematic of the EKINOX-Zr architecture [6]

$$J_{18} = \tau_{18}J_O - C_O D_O \nabla C_{18} \tag{15}$$

In [1], Mishin and Borchardt defined the oxygen tracer flux as the following equation (Eq. (10) p. 867 in [1]):

$$J_O^* = cJ_O - C_O D_O^* \nabla c \tag{16}$$

A one-to-one identification between Eqs. (15) and (16) can be done. J_O^* is the flux of O-tracer, noticed J_{18} in the present work; c is the ratio of O-tracer, corresponding to τ_{18} in the present work; ∇c is the gradient of the tracer concentration, that is to say ∇C_{18} in the present work; and $D_O^* = fD_O$, where the correlation factor f is named f_o and it is equal to the unity.

Thus, when $\left[V_O^{z\bullet}\right] \ll 1$ the Eqs. (15) and (16) are equivalent, this corresponds to the conditions of Mishin and Borchardt's work.

The isotope fluxes in the metallic matrix are governed by the Brownian's motion and are given by Eq. (17). In those two equations, the approximation on the activity coefficient $\gamma_a = 1$ is assumed.

$$\forall i \in \{16; 18\}, J_i = -D_O \nabla C_i \tag{17}$$

Modifications of EKINOX-Zr Model

Detailed presentations of the EKINOX-Zr model are available in [5, 6]. It is reminded that in this model, the fuel cladding tube is modeled as a one-dimensional planar domain divided into n slabs (Fig. 1). The growth kinetics of both the oxide scale and the $\alpha_{Zr}(O)$ layer is calculated by EKINOX-Zr model. A numerical resolution of Fick's equations (thanks to an explicit finite difference algorithm) with boundary conditions on moving interfaces allows determining the penetration profile of oxygen. The interfaces are considered at local equilibrium, and the thermodynamic database Zircobase [10] (CALPHAD formalism) is used to calculate the boundary concentrations.

Given that EKINOX-Zr model is already able to calculate the overall oxygen penetration, one can follow the penetration of each isotope by adding only the

calculation of the penetration of ^{16}O and calculating ^{18}O by the difference. Firstly, it is assumed that the Eq. (18)[4] is valid in the bulk metal (O diffuses as an interstitial) and that the Eq. (19) is valid in the oxide. Then, the whole penetration profile of ^{18}O can be deduced from Eqs. (18) and (19) once the O, ^{16}O, and vacancies concentrations have been calculated by the EKINOX-Zr model.

$$\text{(metal)} \quad \forall p \in \mathbb{N} | 1 \leq p \leq i, X_O^p = X_{18}^p + X_{16}^p \tag{18}$$

$$\text{(oxide)} \quad \forall q \in \mathbb{N} | i + 1 \leq q \leq n, X_O^q = 1 - X_{V_O}^q = X_{18}^q + X_{16}^q \tag{19}$$

A discretized expression of Eq. (17) for the flux J_{16}^p in the bulk metal is given by the Eq. (20). If one defines the diffusion coefficient D_{ox} as $D_{ox} = (1 + a)D_{V_O^{a\bullet}}$, a discretized expression of the Eq. (12) for the flux J_{16}^q can be provided by Eq. (21).

$$\text{(metal)} \quad \forall p \in \mathbb{N} | 1 \leq p \leq i, J_{16}^p = -D_O^p \frac{X_{16}^{p+1} - X_{16}^p}{\frac{e^p + e^{p+1}}{2}} \tag{20}$$

$$\text{(oxide)} \quad \forall q \in \mathbb{N} | i + 1 \leq q \leq n, J_{16}^q = -\gamma^q D_{ox}^q \frac{X_{16}^{q+1} - X_{16}^q}{\frac{e^q + e^{q+1}}{2}} + \tau_{16}^q(1 - \gamma^q)D_{ox}^q \frac{X_{V_O}^{q+1} - X_{V_O}^q}{\frac{e^q + e^{q+1}}{2}} \tag{21}$$

From the Eqs. (20) and (21), it is possible to obtain the evolution of isotopic concentrations as follows:

$$\forall r \in \mathbb{N} \backslash \{j, j+1, i, i+1\} | 2 \leq p \leq n - 1, \frac{dX_{16}^r}{dt} = \Omega^r \frac{J_{16}^r - J_{16}^{r+1}}{e^r} \tag{22}$$

The variations of isotopic concentrations in the slabs around each interface are given by Eqs. (23–28):

$$\dot{X}_{16}^1 = -\frac{J_{16,met}^1}{e^1} \tag{23}$$

$$\dot{X}_{16}^j = \frac{J_{16,met}^{j-1}}{e^j} \tag{24}$$

$$\dot{X}_{16}^{j+1} = -\frac{J_{16,met}^{j+1}}{e^{j+1}} \tag{25}$$

$$\dot{X}_{16}^i = \frac{J_{16,met}^{i-1}}{e^i} \tag{26}$$

$$\dot{X}_{16}^{i+1} = -\frac{J_{16,ox}^{i+1}}{e^{i+1}} \tag{27}$$

---

[4] The superscript p is linked to the metallic slabs whereas the superscript q is linked to the oxide slabs.

$$\dot{X}_{16}^n = \frac{J_{16,\text{ox}}^{n-1}}{e^n} \qquad (28)$$

It is now possible to express the equations of the variation of isotopic concentrations between two time steps:

$$\forall r \in \mathbb{N} \,|\, 1 \le r \le n-1, X_{16}^r(t+\Delta t) = X_{16}^r(t) + \Delta t \frac{dX_{16}^r}{dt} \qquad (29)$$

$$\forall r \in \mathbb{N} \,|\, 1 \le r \le n-1, X_{18}^r(t+\Delta t) = 1 - X_O^r(t+\Delta t) - X_{16}^n(t+\Delta t) \qquad (30)$$

At the oxide/gas interface, the proportion of each isotope changes as a function of the incoming flux of mixed $^{16}O_2/^{18}O_2$ gas. The fraction of ^{18}O isotope in the $^{16}O_2/^{18}O_2$ mixed gas is called R_{18}. Then, the concentrations of ^{16}O and ^{18}O at each time step in the slab n are given by Eqs. (31) and (32):

$$X_{16}^n(t+\Delta t) = X_{16}^n(t) + (1-R_{18})\Delta t \dot{X}_{16}^n \qquad (31)$$

$$X_{18}^n(t+\Delta t) = 1 - X_{V_o}^n(t+\Delta t) - X_{16}^n(t+\Delta t) \qquad (32)$$

As stated before, the oxygen concentrations at the interface are fixed to the equilibrium values. Then, the isotopic concentrations in the slabs 1, j, $j+1$, i, and $i+1$ are fixed to the boundary concentrations as a function of the ratio of each isotope in the slab. For example, the isotopic concentrations in the slab i (metal/oxide interface in $\alpha_{Zr}(O)$) are given by the Eqs. (33) and (34):

$$X_{16}^i(t+\Delta t) = \left(\frac{X_{16}^i(t)}{X_{16}^i(t) + X_{18}^i(t)}\right) C_{\alpha_{Zr}/\text{ox}} \qquad (33)$$

$$X_{18}^i(t+\Delta t) = \left(1 - \frac{X_{18}^i(t)}{X_{16}^i(t) + X_{18}^i(t)}\right) C_{\alpha_{Zr}/\text{ox}} \qquad (34)$$

Results and Discussion

Tables 1 and 2 summarize all the thermodynamic and diffusion data used to perform calculations shown in this part. Please note that in the oxide scale, the boundary concentrations of vacancies and oxygen are defined with reference to the stoichiometry of ZrO_{2-x}. Notice that a constant value for diffusion coefficient of vacancies in the oxide is used as the only input parameter for diffusion in the oxide

Table 1 Oxygen boundary concentrations calculated with ThermoCalc and the Zircobase [10]

T (°C)	$C_{\beta_{Zr}/\alpha_{Zr}}$ (at)	$C_{\alpha_{Zr}/\beta_{Zr}}$	$C_{\alpha_{Zr}/ox}$	$[V_O^{\bullet\bullet}]_{ox/\alpha_{Zr}}$	$[V_O^{\bullet\bullet}]_{ox/gas}$
1200	2.76×10^{-2}	1.15×10^{-1}	3.00×10^{-1}	6.92×10^{-2}	1.00×10^{-8}

Table 2 Oxygen diffusion coefficients used in EKINOX-Zr calculations [11]

T (°C)	$D_{\beta_{Zr}}$ (cm² s⁻¹)	$D_{\alpha_{Zr}}$	$D_{ox} = (1 + \alpha)D_{V_O^{\bullet\bullet}}$	$D_O|_{ox/\alpha_{Zr}}$	$D_O|_{ox/gas}$
1200	1.55×10^{-6}	1.10×10^{-7}	9.36×10^{-7}	2.16×10^{-8}	3.12×10^{-15}

for EKINOX calculation. Considering the gradient of vacancies in the oxide, this leads to variation of the O intrinsic diffusion coefficient across the oxide. Table 2 also gives in the two last columns the corresponding values for O intrinsic diffusion coefficient at ox/α_{Zr} interface and oxide/gas interface.

Figure 2 shows a comparison between Mishin and Borchardt study [1] and EKINOX-Zr calculations. Figure 2 presents two isotopic distribution profiles calculated for the oxidation of zirconium during 1000 s at 1200 °C. The first 500 s corresponds to an oxidation under $^{16}O_2$ (natural stage) and the last 500 s are under $^{18}O_2$ (tracer stage). The total oxygen concentration profile is also depicted in the figure. Hence, one can follow both the growth of the zirconia scale and $\alpha_{Zr}(O)$ layer. The shape of the ^{18}O concentration profiles corresponds to the typical profiles for systems where diffusion takes place only by lattice diffusion. Notice that the ^{18}O distribution profile would be very different in the case of short-circuit contribution [12].

Mishin and Borchardt [1] report that the tracer penetration profile can be fitted by the Eq. (35) where $\overline{D}_O$ is the average chemical diffusion coefficient of the tracer:
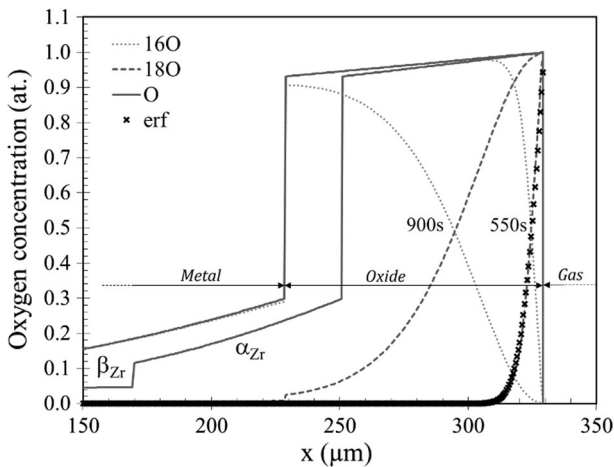

Fig. 2 EKINOX-Zr calculation: two sets of distribution profiles of O, ^{16}O, and ^{18}O plotted for an oxidation of zirconium alloy during 1000 s at 1200 °C, the first stage (500 s) is performed under $^{16}O_2$ while the second stage (500 s) is performed under $^{18}O_2$. Comparison between the analytical solution "erf" (Eq. 38) and the ^{18}O penetration profile calculated by EKINOX-Zr

$$C_{18}(x) = C_{18}^{\text{oxide/gaz}} \text{erf}\left(\frac{x}{2\sqrt{\bar{\bar{D}}_{\text{O}}t}}\right) \tag{35}$$

Following this statement, Fig. 2 presents a comparison between the ^{18}O penetration profile calculated by EKINOX-Zr and the analytical solution of $C_{18}(x)$ given by Eq. (35). The parameters of the analytical formula were chosen as followed: $C_{18}^{\text{oxide/gaz}} = 0.988$ at (equal to the value of X_{18}^n given by EKINOX-Zr calculation), $t = 550$ s (that corresponds to the calculation duration). With an adjusted value of $\bar{\bar{D}}_{\text{O}} = 4.5 \times 10^{-10}$ cm^2 s^{-1} in Eq. (35), a good fit is obtained between the analytical solution and the numerical calculation. Following the Eq. (14), it is possible to calculate the values of $\tilde{D}_{\text{O}}$ close to the oxide/gas interface and at the "end" of the ^{18}O penetration profile. All the values are summarized in Table 3 that clearly shows that the value of $\bar{\bar{D}}_{\text{O}}$ used in the Eq. (35) is consistent with two values of $\tilde{D}_{\text{O}}$ calculated with the Eq. (14).

Initially, the Eq. (35) is provided in [1] to measure the self-diffusion coefficient D_{Oeff} of the oxygen tracer. To do so, authors assumed that the self-diffusion coefficient is constant in the whole oxide scale, even if they clearly mentioned that the self-diffusion coefficient depends strongly on the local vacancy concentration. Finally, they conclude that their assumption is available for short-term oxidation (i.e., in the case when the diffusion is largely predominant over the transport). In the case of zirconium oxidation, if we take a look at the Eq. (14), we can see that close to the oxide/gas interface, because of the very small value of the vacancy concentration; the global diffusion coefficient of the diffusion part (first term in RHS of Eq. 14) is equal to 3.12×10^{-15} cm^2 s^{-1}, whereas the global diffusion coefficient of the transport part (second term in RHS of Eq. 14) is equal to 9.36×10^{-7} cm^2 s^{-1}. Thus, the transport part cannot be neglected even for short-time tracer stage. So, we can say that the Eq. (35) allows us to measure only an average chemical diffusion coefficient and not the self-diffusion coefficient.

The numerical model has also been used to imagine a new type of tracer experiments with a short-time $^{18}\text{O}_2$ stage surrounded by two $^{16}\text{O}_2$ stages of longer durations. Hence, a calculation has been realized considering that the entire oxidation is performed under the natural stage with 100% $^{16}\text{O}_2$ except between 200 and 230 s when the tracer stage is performed under 100% $^{18}\text{O}_2$.

Table 3 Comparison between the values of $\tilde{D}_{\text{O}}$ calculated with the Eqs. (14) and (35)

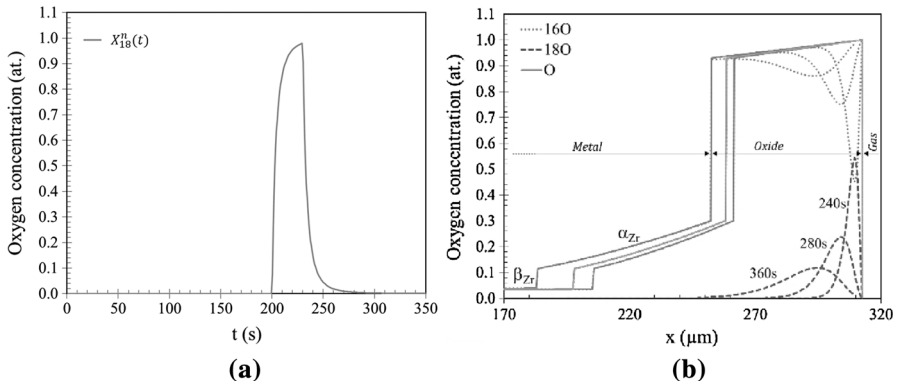| X (µm)	280 "End of ^{18}O profile"	320-329 $\bar{\bar{D}}_{\text{O}}$	329 Oxide/gas interface
Calculated from	Eq. (14)	Eq. (35)	Eq. (14)
$\tilde{D}_{\text{O}}$ (cm^2.s^{-1})	1.4×10^{-8}	4.5×10^{-10}	3.1×10^{-10}

Fig. 3 a Time evolution of ^{18}O concentration in the first numerical slab of oxide. b Isotope diffusion profiles calculated at 240, 280 and 360 s by EKINOX-Zr for an oxidation of zirconium containing a 30 μm prior-oxide layer. The following sequences have been ordered as follows: 200 s under ^{16}O$_2$ → 30 s under ^{18}O$_2$ → 970 s under ^{16}O$_2$. For a better understanding, we chose to set all the oxide/gas interfaces at the same abscissa

Table 4 Values of $\tilde{D}_O$ measured by following the ^{18}O peak displacement from Fig. 3. The maximum value of the ^{18}O at the oxide/gas interface is reached for $t = 230$ s

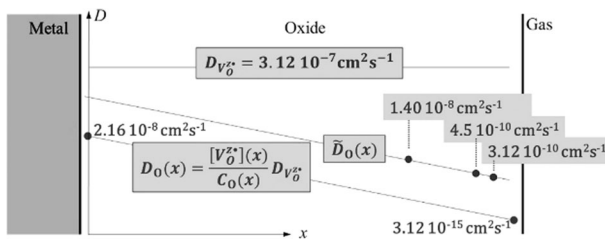| t (s)	240	280	360
Δt (s)	10	50	130
Δx (μm)	3	8.6	18
$\tilde{D}_O$ (cm^2 s^{-1})	9.0×10^{-9}	1.5×10^{-9}	2.5×10^{-8}

Fig. 4 Schematic illustration of the evolution of each diffusion coefficients along the oxide scale

Figure 3a shows the time evolution of the concentration of ^{18}O in the first numerical slab of oxide besides the oxide/gas interface, that is to say the evolution of ^{18}O concentration at the oxide scale surface for this specific calculation. The evolution of ^{18}O concentration at the surface results from the Eqs. (31) and (32) which differ from the drastic assumption usually made by imposing a constant surface concentration. Figure 3a shows that the enrichment in ^{18}O at the oxide surface is rapid and the maximum value is reached 30 s after the introduction of ^{18}O$_2$ in the atmosphere. Figure 3b shows the evolution and displacement of the peak of ^{18}O tracer for three different durations. The evolution of the ^{18}O distribution

profiles illustrates both contributions: diffusion and transport. The transport term induced the inward displacement of the ^{18}O peak position in the oxide scale while the diffusion term induced the spreading of the O peak with time.

If one follows the abscissa of the summit of the ^{18}O peak as a function of time, we can obtain values of $\tilde{D}_O$ considering that $\Delta x = \sqrt{\tilde{D}_O \Delta t}$ [13]. The values are summarized in Table 4.

Table 4 shows the same evolution of $\tilde{D}_O$ than in Table 3. Tables 3 and 4 clearly show that $\tilde{D}_O$ is increasing from the oxide/gas interface to the metal/oxide interface, as for D_O. This is due to the increase of the vacancy concentration.

Figure 4 presents a schematic illustration of the evolution of each diffusion coefficient. We can see that all the values are consistent with each other. Furthermore, Fig. 4 shows that the assumption made in [1] on the constant value of the self-diffusion coefficient is not relevant in the case of zirconium oxidation.

Conclusions

In this work, our aim was to simulate O-tracer experiments at high temperature taking into account a high oxygen solubility limit of oxygen in the metal. A second objective was to obtain a numerical model able to simulate any kind of tracer diffusion during the oxidation, even in non-stationary regimes. The diffusion equations of ^{16}O and ^{18}O were deduced from classical diffusion equations taking into account the electrochemical potential gradient across the oxide scale through the large gradient of anionic vacancy concentration. The numerical implementation of these equations in the existing EKINOX-Zr model enabled direct calculation of isotope fluxes without making the approximation of a constant oxygen intrinsic diffusion coefficient which was done in Mishin and Borchardt's work [1]. Indeed, the oxygen diffusion coefficient is proportional to the local vacancy concentration; therefore, it is best to use a flux equation expressed as a function of a constant diffusion coefficient of the oxygen vacancies. Two examples of numerical calculations illustrated how the shape of the ^{18}O-tracer distribution profile is governed by both the diffusion by Brownian motion and the transport under the large gradient of defects through the growing oxide scale.

Firstly, the simulation of a classical two-stage tracer experiment is consistent with the analytical solution given in [1]. The average value of $\overline{\tilde{D}_O}$ used in the Eq. (35) is clearly included between the two values of $\tilde{D}_O$ obtained from the Eq. (14). Despite what is reported in [1], in the case of zirconium oxidation, the transport contribution cannot be neglected in the isotope flux expression, even for short-term oxidation.

Secondly, a new type of O-tracer experiment is proposed to evaluate oxygen chemical diffusion and transport contributions from the drift of a ^{18}O peak. In this case, the values of $\tilde{D}_O$ were calculated using the peak drift. The values of $\tilde{D}_O$ obtained by this way and reported in Table 4 are consistent with the one reported in Table 3. By three different ways of calculation, all the values of $\tilde{D}_O$ are consistent

with each other. Thus, we can conclude that the "peak shift" method together with Eq. 14 should be used to determine the values of oxygen diffusion coefficient in growing oxide scales.

Next step to improve the EKINOX-Zr will be to express the flux as a function of the gradient of the local chemical potential gradients calculated using the thermodynamic database Zircobase [11]. This improvement would avoid the strong assumption of the constant value of the coefficient of activity in the metal. For example, thermodynamic calculations show that in $\alpha_{Zr}(O)$ the activity coefficient evolves over two order of magnitude.

References

1. Y. H. Mishin and G. Borchardt, *Journal of Physics III France* **3**, 1993 (863).
2. S. Chevalier, G. Strehl, J. Favergeon, F. Desserrey, S. Weber, O. Heintz, G. Borchardt and J.-P. Larpin, *Materials at High Temperature* **20**, 2003 (253).
3. R. Tricot, *Techniques de l'Ingénieur* M2360 (1994).
4. C. Toffolon-Masclet, C. Desgranges. C. Corválan-Moya, J.-C. Brachet. *Solid State Phenomenon* **172–174**, 652 (2011).
5. B. Mazères, C. Desgranges, C. Toffolon and D. Monceau, *Oxidation of Metals* **79**, 2013 (121).
6. B. Mazères, C. Desgranges, C. Toffolon and D. Monceau, *Corrosion Science* **103**, 2016 (10).
7. G. Petot-Ervas, D. Monceau and C. Petot, *Ceramic Transactions* **24**, 1991 (113).
8. P. Kofstad, *High Temperature Corrosion*, (Elsevier Apllied Science Publishers LTD, London, 1988), pp. 164–168.
9. H. Schmalzried, *Chemical Kinetics of Solids.* Eds: (Wiley, VCH Verlag GmbH, 1995).
10. N. Dupin, I. Ansara, C. Servant, C. Toffolon, C. Lemaignan and J.-C. Brachet, *Journal of Nuclear Material* **275**, 1999 (287).
11. X. Ma, C. Toffolon-Masclet, T. Guilbert, D. Hamon and J.-C. Brachet, *Journal of Nuclear Materials* **377**, 2008 (359).
12. G. Bakradze, L. P. H. Jeurgens, T. Acatürk, U. Starke and E. J. Mittemeijer, *Acta Materialia* **59**, 2011 (7498).
13. J. Philibert, *Diffusion et transport de matière dans les solides*, (Les Editions de Physique, Paris, 1990), pp. 5–11.